ANALYSIS and DEVELOPMENT of FAN NOISE PREDICTION METHODOLOGY

Shedolkar Pravinkumar

A Thesis Submitted to

Indian Institute of Technology Hyderabad

In Partial Fulfillment of the Requirements for

The Degree of Master of Technology

भारतीय प्रौद्योगिकी संस्थान हैदराबाद
Indian Institute of Technology Hyderabad

Department of Department of Mechanical and Aerospace Engineering

July 16, 2015

Declaration

I declare that this written submission represents my ideas in my own words, and where ideas or words of others have been included, I have adequately cited and referenced the original sources. I also declare that I have adhered to all principles of academic honesty and integrity and have not misrepresented or fabricated or falsified any idea/data/fact/source in my submission. I understand that any violation of the above will be a cause for disciplinary action by the Institute and can also evoke penal action from the sources that have thus not been properly cited, or from whom proper permission has not been taken when needed.

(Signature)

(Shedolkar Pravinkumar)
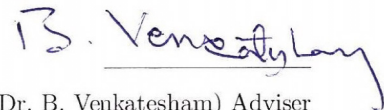
ME13 M1013

(Roll No.)

Approval Sheet

This Thesis entitled Analysis and development of fan noise prediction methodology by Shedolkar Pravinkumar is approved for the degree of Master of Technology from IIT Hyderabad
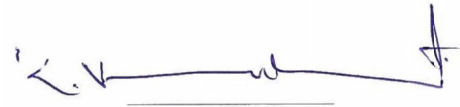
(Dr. Narasimha Mangadoddy) Examiner
Dept. of Chem Eng
IITH

(Dr. Raja Banerjee) Examiner
Dept. of MAE
IITH

(Dr. B. Venkatesham) Adviser
Dept. of MAE
IITH

(Dr. K. Venkata Subbaiah) Co-Adviser
Dept. of MAE
IITH

(Dr. Narasimha Mangadoddy) Chairman
Dept. of Chem Eng
IITH

Acknowledgements

Dedication

To my family and to everyone who has been part of my learning experiences.

Abstract

A widespread industrial application of centrifugal fans has been found in literature. The centrifugal fans have been widely adopted by domestic, industrial applications and electronic industries due to their large capacity of mass flow and their compactness. It has pointed out that many machines having a moderate efficiency and low aero-acoustic performances are still in operation and could certainly be improved by making use of todays technology. Prediction of noise generated by centrifugal fans is much more complex, and it is a multi-physics problem. An integrated approach has to be considered for estimating aerodynamic forces, acoustic analogies and aero-acoustics simulation. Prediction of fan noise at design stage helps to select quieter fan and operate at higher efficiency. Fan curve is an initial step in selecting a fan for a given system. However, many times it is not easily available. A methodology has been developed to estimate fan curve using computation fluid dynamic simulations (CFD). Present methodology and results have been validated with results available in the literature. Unsteady flow characteristics and associated aero acoustics blade tonal noise of a cross-flow fan has been predicted by incompressible flow simulations. The three-dimensional incompressible Navier Stokes equations in a moving coordinate system has been solved by an unstructured finite-volume method. Polyhedral meshes and sliding mesh techniques are utilized to model the interface between rotating and stationary domains. Different turbulent models have considered in simulations to suggest an appropriate model for centrifugal fans. Equivalent noise sources have estimated with the computed aerodynamic forces based on the Ffowcs Williams and Hawkings equation. Wave propagation equations have solved to predict sound radiation. A centrifugal fan with 12 blades with inlet and outlet ducts, and two different operating speeds have been considered for the simulation. Acoustic simulations have done in a frequency domain up to 5000 Hz. It could capture until 20 harmonics for 2000 RPM and eight harmonics for 5000 RPM. The simulated results have analyzed to understand the role of turbulent kinetic energy, vorticity pattern in noise generation. A parametric study by changing inlet velocity, cut off radius and number of blades have done. Validation of the present method has been made by comparing fan curve generated by numerical solution to the general fan curve equations and predicted noise results have compared with available empirical equations in the literature. Parametric studies have been done to estimate the sound pressure level as a function of inlet flow rate. This data might help to estimate of efficient operating conditions for a fan.

Contents

Abbreviations

CFD - Computational Fluid Dynamics

FWH - Ffowcs Williams and Hawkings

VIV - Vortex Induced Vibration

TKE- Turbulent kinetic energy

IT- Incident Turbulence

TBTE-Turbulent Boundary layer / Trailing Edge interaction

TBS- Turbulent boundary layer / Blade Surface interaction (TBS)

FS- Flow Separation

Nomenclature

k - Turbulent kinetic energy

ϵ- Turbulent dissipation rate

P_{loss} - Pressure loss

W - overall radiated sound power

u_2- Circumferential velocity at impeller's outer diameter

a- is speed of sound

M - Mach number

$\dot{V}$ - Volume flow rate

Δp_t - Total Pressure rise

η -efficiency

λ - wave length

$\overline{p^2}$-Mean square pressure difference fluctuation

A_c-correlation area

c-Blade chord

Λ-Turbulent eddies

w-Turbulent velocity fluctuation

U-Local mean velocity

ρ-density

ϕ-lift curve slope

Q- Volume flow rate

P_d -Pressure drop

C- Correction factor related to efficiency

K_w -Octave Band Sound power level Correction Factor for Fans

K-wave number

ρ_0 - constant density

$\rho^{'}$ - density fluctuation

List of Figures

3

List of Tables

Chapter 1

Introduction

Prediction of noise generated by fan is more complex process. A complete, aerodynamic and aero acoustic, investigation of the tonal noise of a high rotational speed centrifugal fan is the aim of my thesis work. The purpose of this work is to understand the nature of noise generated in a fan. An aero acoustic model based on the Ffowcs Williams and Hawkings equation is used to predict noise numerically.

When talking about acoustics, most people relate it to music. However, music, joyful sound, is not the only important aspect in acoustics. Acoustic noise is a major concern of society and industry, and aerodynamic or flow noise is especially concerning because it is closely related to the level of comfort of the environments in which people live and work. Common examples of aerodynamic noise are jet noise and noise generated when the fluid flows over obstacles and cavities. The prediction of sound generated from fluid flow has always been a difficult subject due to the nonlinearities in the governing equations. However, flow noise can now be simulated with the help of modern computation techniques and super computers.

Aerodynamic noise is a result of unsteady gas flow and the interaction of the unsteady gas flow with the associated structure. The unwanted gas flow and structure interaction may cause serious problems in industrial products such as the instability of the structures and structure fatigue [4] . Accordingly, simulating the aerodynamic noise is necessary and at the design stage. However, due to the nature of turbulent flow and the limitation of computational power, it is not always feasible to obtain a reliable unsteady (transient) CFD solution for the aerodynamic noise analysis. The computational effort and time is a major hindrance. Even if there were no time limitation, any one of the commonly used turbulent models is not capable of solving all scales of turbulence[5]. Therefore, a time-efficient method with acceptable accuracy is needed in order to estimate flow noise. Several well-known theories such as the theory of Lighthill [6] and the theory of Ffowcs Williams and Hawkings (FWH) [7] have been successfully applied to aero acoustic problems. The theory of Lighthill is the foundation of the FWH approach. In Lighthills paper, it has been shown that aerodynamic sound sources can be modeled as series of monopoles, dipoles, and quadruples generated by the turbulence in an ideal fluid region surrounded by a large fluid region at rest (i.e., velocity field in the fluid is zero).

In Lighthills analogy, no fluid flow and sound wave interaction is considered. A justification of this assumption has been given in Lighthills original paper. Due to the large difference in energy,

there is very little feedback from acoustics to the flow. Commercial codes such as STAR CCM+ (CD-adapco) and LMS virtual lab have incorporated the FWH approach in a computational aero acoustics module. FWH assumes that there are no obstacles between the sound sources and the receivers [7]. Therefore, the sound radiation problem is inherently a weak part of the simulation, especially if the sound source is in a waveguide or duct, enclosed, or obstructed in some way.

This thesis examines the combination of the CFD solvers and the boundary element technique for the prediction of sound radiated from turbulent flow in centrifugal fan.

1.1 Objectives

Objective of is

1. Development of methodology and identification of appropriate model for fan noise prediction.

2. Integration of CFD and acoustic models.

3. The Fan curve estimation including noise prediction.

This study used the commercial code STAR CCM + as CFD solver and LMS VL as the acoustic wave solver. The sound power generated in process computed and compared to the theoretical or empirical solutions available in literature.

1.2 Motivation

Sources of noise in common appliances.

1. Household sources: Appliances like food mixer, grinder, vacuum cleaner, washing machine and dryer, cooler, air conditioners, can be very noisy and injurious to health.

2. Commercial and industrial activities: Printing presses, manufacturing industries, construction sites, contribute to noise pollutions in large cities.

3. Transportation: aero planes, trains, vehicles on roadthese are constantly making a lot of noise and people always struggle to cope with them.

70 % of worlds noise is due to rotating bodies and 60% of that is due to fan and still there is no robust methodology which can predict tonal and broadband noise. Noise induced by flow over obstacles and flow inside rotating body are common engineering problem. In most instances, vortex - turbulence is the major culprit. Of course, vortex induced vibration (VIV) is well known to cause serious engineering failures (such as structure fatigue). Accordingly, it will be beneficial to use simulation, engineers can make modifications to a design in a virtual environment and avert serious aero acoustic problems.

An outline of the thesis chapters :

- Chapter 2 gives a literature review of previous work done in developing CFD and acoustic models.

- Chapter 3 is about acoustic sources.

- Chapter 4 is about numerical modelling and fan performance.

- Chapter 5 is about parametric study.

- Chapter 6 concludes results.

Chapter 2

Literature survey

2.1 CFD Literature survey

A number of previous projects have been done using different CFD model to simulate rotating bodies.

Pericleous and Patel(1986) developed a mathematical model for simulation of tangential and axial agitators in chemical reactors. Impellers were represented as a quadratic source of momentum in the tangential and/or axial directions (depending on the type of impeller); while the other geometries, such as the baffles, were represented as sinks of momentum. The lift and drag coefficients from experimental data of the blade cross-sectional airfoil profiles were used to calculate the blade forces. The momentum contributions from these forces were then introduced as appropriate momentum sources and sinks in the Navier-Stokes equations and solved using a control volume formulation. Good agreement was found, but the model showed some inadequacy in modelling turbulence.

Pelletier and Schetz (1986) and Schetz et al. (1988) investigated the three dimensional flow in close vicinity of a propeller. Turbulence modelling was achieved through a generalization of an integrated turbulent-kinetic-energy model. The general purpose finite element fluid dynamics program FIDAP was used to program the turbulence model. Good agreement was found in comparison with wind tunnel measurements for the prediction of velocity and pressure profiles along the radial axis.

Thiart and von Backstrm (1993) developed an actuator disk model for a low solidity/low hub-to-tip ratio axial flow fan. The Navier-Stokes equations were solved with the aid of a $k - \epsilon$ turbulent model and the SIMPLEN method.

Van Staden (1996) integrated a fan performance model into a CFD model for the performance prediction of a complete air-cooled condenser. Experimental fan performance curves were used to obtain the momentum source term of the fan in the axial direction, which was added to the Navier-Stokes equation as a source term in the CFD model. Good agreement was found with experimental data at ideal conditions, but for non-ideal conditions (such as distorted in flow) the model required the fan performance curves at these adverse conditions.

Kelecy (2000) predicted the fan performance of a four-bladed axial flow propeller over a range of flow rates and compared the results with wind tunnel data. The blade has a rotational speed of 2000 rpm and a diameter of 0.11 m. The rotating reference frame method of commercially available software FLUENT was used to simulate the rotation of the $\frac{1}{4}^{th}$ axisymmetric fan model. The flow

equations were solved in rotating frame. A zero velocity was imposed on blade surfaces and shaft, while the outer walls of the tunnel were rotated at specified speed in the opposite direction when viewed from stationary reference frame.

A complete three-dimensional CFD model was used by Ramasubramanian et al. (2008) to analyses the fiber diffusion process in the manufacturing of wet-laid nonwovens. The three-bladed impeller and baffles were modelled in commercially available software FLUENT by using the MIXSIM user interface and incorporating the multiple reference frame model. This meant that for the impeller a rotating reference frame was used and for the baffles and tank, a stationary reference frame was used. The impeller has a diameter of 0.2 m and rotates at 350 rpm. A standard $k - \epsilon$ turbulence model was used for the flow solution. Simulation results was compared to experimental work on a mixing tank with baffles and an impeller located at center of the tank. The author found the model useful to predict the location, sources and mechanism behind the formation rope and defects.

A complete three dimensional centrifugal fan performance study given in reference [8].Author have created experimental fan curve and validated with fan curve generated from numerical solution. Parametric study of centrifugal fan performances showed that increase in the number of blades increases the flow coefficient accompanied by an increase in power coefficient. Increase in the number of blades increases the flow coefficient and efficiency due to better flow guidance and reduced losses.

2.2 Acoustic Literature survey

A good amount of literature is available to predict aerodynamic noise produced by rotating blades in low Mach number, low to medium speed axial and centrifugal flow fans with an emphasis on broad band noise. Following LOWSON[9] classified noise prediction methods into three groups:

- Class I: Predictions giving an estimate of overall level as a simple algebraic function of basic machine parameters

- Class II: Predictions based on separate consideration of the various mechanisms causing fan noise, using selected fan parameters

- Class III: Predictions utilizing full information about the noise mechanisms related to a detailed description of geometry and aerodynamics, e.g. they require computation of local blade element velocities and angles of attack.

The objective of current thesis work to develop class III prediction methodology for centrifugal fan. Noise generation due to the fluctuating forces on the fan blades is only considered in the current research work. The most important mechanisms are

- periodically unsteady blade force due to inflow distortions (spatially nonunion inflow, unsteady inflow)

- stochastically unsteady blade forces due to incident turbulence (IT), turbulent boundary layer / trailing edge interaction (TBTE), turbulent boundary layer / blade surface interaction (TBS) and flow separation (FS).

2.3 Prediction Methods

2.3.1 Class I

According to REGENSCHEIT [10] the overall radiated sound power W of a fan is proportional to the aerodynamic losses P_{loss} in the fan and a measure for the flow velocity in the fan

$$W \propto P_{loss}.\left(\frac{u_2}{a}\right)^m$$

Where u_2 is the circumferential velocity at the impeller's outer diameter D_2, a,is the speed of sound, and m is Mach number exponent which has to be determined experimentally but is assumed to be constant for a given type of fan (centrifugal, axial, etc.). If the losses are expressed by the overall performance data of the fan (flow rate $\dot{V}$, total pressure rise Δp_t and efficiency η) one obtains

$$W \propto \left[\frac{\dot{V}}{\eta} - \dot{V}\Delta p_t\right].\left(\frac{u_2}{a}\right)^m = \left[\dot{V}\Delta p_t\left(\frac{1}{\eta}-1\right)\right].\left(\frac{u_2}{a}\right)^m$$

2.3.2 Class II

SHARLAND's method [11] is fundamental for many later studies on fan noise and therefore described briefly. His starting point is a flow containing rigid surface under the assumption of acoustic compactness (characteristic dimensions of the surface $<<\lambda$) which radiates into the free field due to pressure fluctuations over the surface:

$$W = \frac{\omega^2}{12\pi\rho a^3}\int\int_S \overline{p^2}A_c\,dx_1\,dx_2$$

Where $\overline{p^2}$ is mean square pressure difference fluctuation , thought of as a local lift fluctuation per unit area a (thus the integration is over only one side of the closed surface S), A_c the correlation area. From that SHARLAND derives working equations for the three noise mechanism IT, TBTE and TBS; e.g for IT under the assumptions that

- the blade chord c is much smaller than the size of the approaching turbulent eddies Λ

- the turbulent velocity fluctuation w normal to the surface is much smaller than the local mean velocity U parallel to the surface

and with lift curve slope ϕ such that $C_L = \phi_w U$, here $\phi = 0.9\pi$ and correlation area $A_c = \frac{U^2}{\omega^2}$ (from former turbulence investigation) he obtains

$$W = \frac{\rho}{48\pi a^3}\int_H \phi^2 U^4\overline{w}^2 C\,dx_2$$

The entire method requires the local mean velocity U parallel to the blade surface and the velocity fluctuations of the incidence turbulence w^2 as aerodynamic input parameters. However, due to the assumptions and simplifications this method does not yield any frequency information of the radiated sound power these models which are based on as single surface in a flow be applied to a rotating fan rotor , As shown by MORFEY et al. [12] the sound spectrum of a rotating broad band source is unaffected by its rotation, i.e. by the Doppler shift. Duct walls, intake bells and other reflecting surfaces may not influence the overall radiated power as long as their representative dimensions are comparable with, or greater than,$\lambda/4$, i.e. if the acoustic radiation is at relatively high frequency [13]. Further, assuming mutually incoherent radiation from each blade, the sound power has just to be multiplied by the number of blades on the rotor.

2.3.3 Empirical Formulae for Sound Power Level Estimation of Fan

$$L_w = K_w + 10logQ + 20logP_d + C \tag{2.1}$$

Where

Q = Volume flow rate in CFM.

P_d =Pressure drop in inches of water.

C= Correction factor related to efficiency.

K_w= Octave Band Sound Power Level Correction Factors for Fans.

By using Fan laws mentioned in chapter 4, L_w can be written in following form.

$$L_w = K_w + 70logD + 50logN + C$$

Table 2.1 gives Octave Band Sound Power Level Correction Factors for forward and backward curved centrifugal fan in FPS units. Whereas table 2.2 gives in MKS units.

Q = Volume flow rate in m3/s.

P_d =Pressure drop in Pascal.

C= Correction factor related to efficiency.

K_w= Octave Band Sound Power Level Correction Factors for Fans.

Forward curve centrifugal fan implies both direction of rotation and blade curvature in same direction.

Table 2.1: Octave Band Sound Power Level Correction factor for Centrifugal Fan(Hz)

Fan type	Charectristics	Octave band Center frequency (HZ)								
		63	125	250	500	1000	2000	4000	8000	BFI
Centrifugal	backward curved Over 36 inch diameter	40	40	39	34	30	23	19	17	3
Centrifugal	backward curved under 36 inch diameter	45	45	43	39	34	28	24	19	3
Centrifugal	forward curved under 36 inch diameter	53	53	43	36	36	31	26	21	2

Table 2.2: Octave Band Sound Power Level Correction factor for Centrifugal Fan (Hz) (in MKS unit)

K_w								
63	125	250	500	1000	2000	4000	8000	BFI
98	98	88	81	83	85	71	66	2

K_w values in MKS unit has given in Table 2.2 where as

Table 2.3: Efficiency correction C

Percentage of Peak Static Efficiency	dB
90-100	0
85-89	3
75-84	6
65-74	9
55-64	12
50-54	15

Table 2.3 gives value of efficiency correction factor C which depend upon efficiency of given fan. These formulae do not include effect of number of blades effect of curvature and other specific details of blades.

Chapter 3

Acoustic sources

Lighthill [6] identified three categories of sound sources due to flow: monopoles, dipoles, and quadruples. Monopoles results from a fluctuating volume or mass flow. Dipoles can form when there are fluctuating forces. When fluctuating forces or dipole. Although higher order poles do exist in aero acoustic problems, they are usually not considered because of their low radiated power.

3.1 Monopole

A monopole radiates sound equally in all directions and is the simplest acoustic source. In aero acoustics, monopoles normally result from pulsating flow. Examples include tire, and compressor noise. One example of a monopole source is a pulsating sphere. Likewise, a loudspeaker can be approximated as a monopole source at low frequencies. The particle velocity of a monopole in the radial direction is given by[6]

$$u(r,t) = \frac{\tilde{A}}{\rho_0} \left(1 + \frac{1}{ikr}\right)^2 e^{i(\omega t - kr)} \tag{3.1}$$

where $\tilde{A}$ is the amplitude [kg/s2],k is the wave number, ρ_0 is the density of the medium, a is the speed of sound in the medium, and ω is the angular frequency. If the monopole source has an infinitely small radius, the volume flow rate can be obtained by taking the limit of the product of the surface area and the particle velocity when the radius goes to zero which yields

$$\tilde{Q} = \frac{4\pi\tilde{A}}{i\omega\rho_0} \tag{3.2}$$

Therefore, the sound pressure for a simple monopole source at a distance r is given by

$$p(r,t) = i\rho_0\omega\frac{\tilde{Q}}{4\pi r}e^{i(\omega t - kr)} \tag{3.3}$$

3.2 Dipole

A dipole is the superposition of two monopoles that are out of phase as shown in Figure 3.1. In aero acoustics, dipoles are normally the result of vortex shedding and fluid structure interaction.
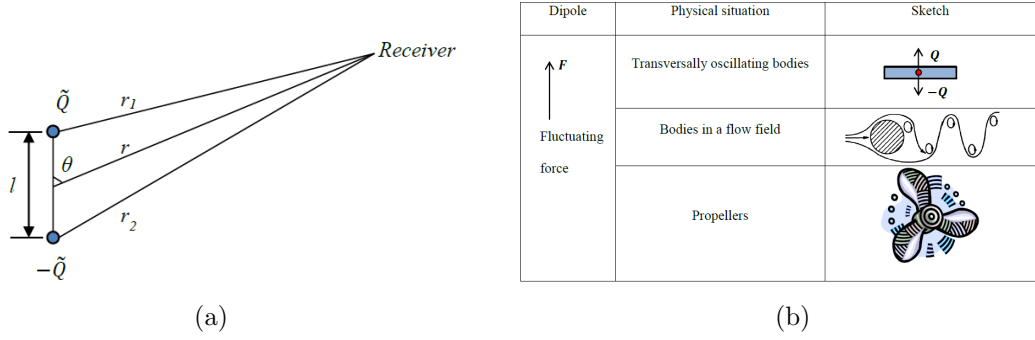
Figure 3.1: (a)Dipole Obtained by Superposition of two Monopoles ($kl\ll1$)(b)Generation of Dipoles (Reproduced [1])

Examples include flow over a rod or cavity.

The sound pressure at the receiver is obtained by adding the sound pressure generated by the monopoles at out-of-phase and can be expressed as

$$p = \frac{\rho_0 i\omega \tilde{Q}}{4\pi}\left(\frac{e^{-ikr_1}}{r_1} - \frac{e^{-ikr_2}}{r_2}\right)e^{i\omega t} \tag{3.4}$$

By utilizing the law of cosines, with the limit of l goes to zero, the sound field induced by the simple dipole can be expressed as

$$p = \frac{ikF cos\theta}{4\pi r}\left(1 + \frac{1}{ikr}\right)^2 e^{-i(\omega t - kr)} \tag{3.5}$$

where

$$F = \tilde{Q}l$$

and $\tilde{Q}$ is the volume flow rate and l is the distance between the two out-of-phase monopoles. It can be seen that dipole sources are induced by forces instead of volume changes in monopoles. In turbulent flow fields, the fluctuating pressure creates a distribution of dipoles at the surface of the body breaking the flow [?]. Figure 3.1 gives example of the physical situations that give rise to dipole sources at low frequencies.

3.3 Quadruples

Similar to the formation of a dipole source, a simple quadruple source can be obtained by the superposition of two dipole sources of the same strength that are out-of phase. Quadruples arise from turbulence. One example is the jet stream. Depending on the distribution of the dipoles, quadruples can be further classified as longitudinal and lateral. Quadruple sources are induced by fluctuating moments or viscous forces. Figure 3.4 and 3.5 shows sound sources and their analogy. Monopole source is like person jumping in still water, water waves radiates equally in all direction. Second case shows dipole behavior two people playing with heavy ball. Whereas third picture in figure 3.5 where two person fighting with each other depicts quadruple source.
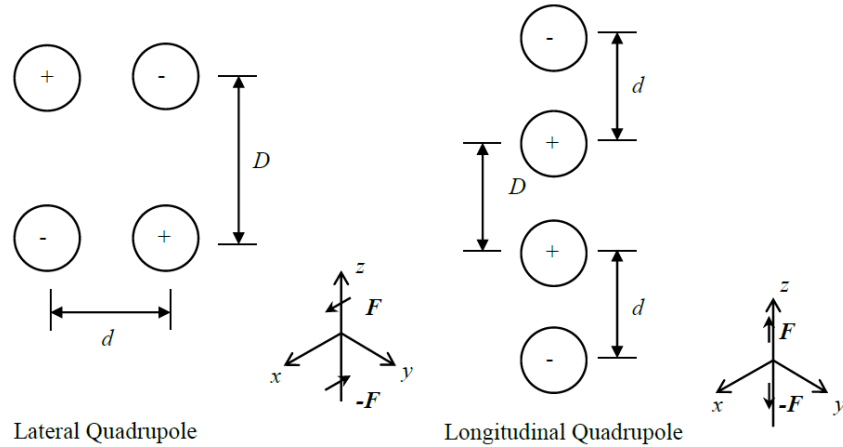
Figure 3.2: Superposition of dipoles

3.4 Vortex shedding

In aero acoustics, unwanted tones are usually caused by vortex shedding. As seen in Figure 3.5, vortex induced noise can be found in many locations around a vehicle body. At (a) type locations such as the windshield base and front hood edge, abrupt changes in body geometry occur. At (b) type locations such as door gaps, air flows over cavities. At (d) type locations such as the radio antenna, air flows over a cylinder. Separated flow exists at each of these locations and vortex shedding may occur depending on the flow conditions. Vortex shedding has been studied since the late 1800s.As shown in Figure 3.6 When viscous fluid flows over solid objects, a boundary layer of fluid around the object will develop. These boundary layers can be either laminar or turbulent which can be determined by local Reynolds numbers. Because of the effects of adverse pressure gradient and the surface viscous stagnation, the flow at the boundary suffers from constant deceleration. Eventually the inertial force is unable to overcome the resistance, and a boundary layer will start to separate from the surface of the object. With the help of the main stream flow, the separated boundary layer will form a pair of vortices rotating in opposite directions. The two vortices shed off alternately and a vortex street forms as the separations occur continuously behind the object, such as a circular cylinder. A relatively steady vortex street formed after a circular cylinder has the following relation [14]:

$$\frac{h}{a} = 0.281 \tag{3.6}$$

where h and a are shown in Figure 3.6 The vortex shedding frequency can be obtained from Equation

$$\frac{fd}{U} = 0.198 \left(1 - \frac{19.7}{Re} \right) \tag{3.7}$$

Where
f, Vortex shedding frequency,
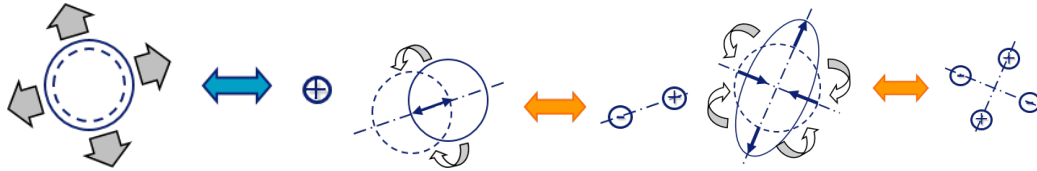d, Diameter of the cylinder,
U, Flow velocity.

15

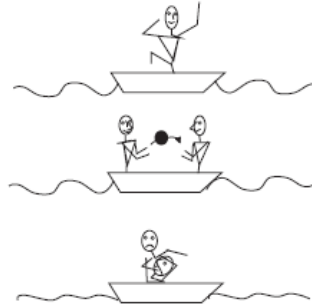Figure 3.3: Monopole Source,Dipole Source, Quadruple Source

Figure 3.4: Monopole, dipole and quadruple generating waves on the surface of the water around a boat.[LMS virtual lab manual]

It is important to understand the vortex regimes of fluid flow across obstacles in order to select the more appropriate laminar or turbulent models. Some turbulence models are only suitable for high Reynolds number flows while others are suitable for low Reynolds flows. Lienhard [15] categorizes the flow regimes for different ranges of Reynolds number. When Re < 5, the flow is laminar and there is no vortex shedding. As the Reynolds number increases, vortices start to appear in the flow field. When Re is in the range of 5 to 15, a fixed pair of vortices first appears in the wake of the cylinder. As the Reynolds number increases to about 40, the former fixed pair of vortices becomes stretched and unstable and as a result, the first periodic driving forces begin. Laminar vortex streets appear when Reynolds number is in the range of 40 to 150. The vortices are laminar till Reynolds numbers exceed roughly 150. For Reynolds numbers above 300, the flow will begin to transition from laminar to turbulent until flow is fully turbulent between roughly 300 and 3105. Another transition takes place when Reynolds numbers in the range of 1105 and 5105. The exact Reynolds numbers for these transitions will vary depending on the surface roughness and the free-stream turbulence level. Although some of the regimes can be further divided into sub categories, the listed regimes and Reynolds number ranges are sufficient to serve as guidelines for the us to select the turbulence models in CFD simulation.

3.5 Acoustic Analogy

3.5.1 Lighthill's analogy

In 1952, a paper named on sound generated aerodynamically, I [6] general theory by Dr. Michael James Lighthill was published. In this paper, he derived a set of formulas which were later named after him. Researchers in acoustics often regard the first appearance of his theory as the birth
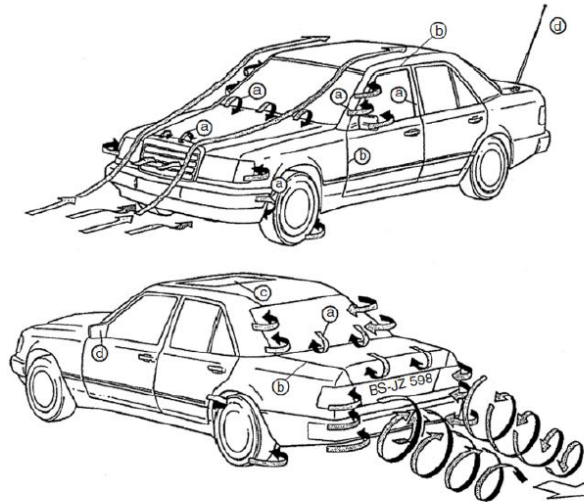
Figure 3.5: Locations of Sound Sources on an Automobile Body [2]
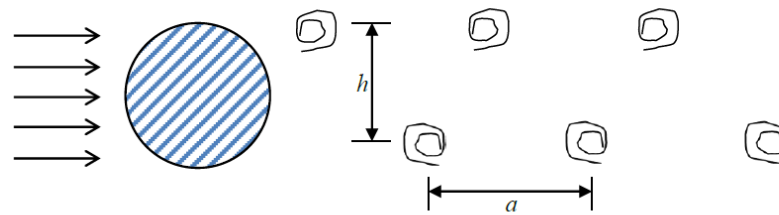
Figure 3.6: Vortex Street after a Cylindrical Obstacle

of aero acoustics. Thereafter, aero acoustics has become a branch of acoustics which studies the sound induced by aerodynamic activities or fluid flow. In 60 years of time, the theory of aero acoustics has been greatly developed and widely applied in modern engineering fields. The subject of Lighthills paper is sound generated aerodynamically, a byproduct of an airflow and distinct from sound produced by vibration of solids. The general problem he discussed in the paper was to estimate the radiated sound from a given fluctuating fluid flow.

There are two major assumptions.

1. Acoustic propagation of fluctuations in the flow is not considered.

2. Preclusion of the back-reaction of the sound produced on the flow field itself. Therefore, the effects of solid boundaries are neglected.

However, the back-reaction is only anticipated when there is a resonator (i.e. a cavity) close to the flow field. Accordingly, his theory is applicable to most engineering problems. Furthermore,

his theory is confined in its application to subsonic flows, and should not be used to analyze the transition to supersonic flow. Lighthill examined a limited volume of a fluctuating fluid flow in a very large volume of fluid. The remainder of the fluid is assumed to be at rest. He then compared the equations governing the fluctuations of density in the real fluid with a uniform acoustic medium at rest, which coincides with the real fluid outside the region of flow. A force field is acquired by calculating the difference between the fluctuating part and the stationary part. This force field is applied to the acoustic medium and then acoustic metrics can be predicted away from the source by solving Helmholtz equation. Helmholtz equation can be solved easily if a free field is assumed or can be solved using numerical simulation. There are two significant advantages in this analogy as mentioned in his paper. First, since we are not concerned with the back-reaction of the sound on the flow, it is appropriate to consider the sound as produced by the fluctuating flow after the manner of a forced oscillation. Secondly, it is best to take the free system, on which the forcing is considered to occur, as a uniform acoustic medium at rest. Otherwise, it would be necessary to consider the modifications due to convection with the turbulent flow and wave propagation at different speeds within the, which would be difficult to handle. Using the method just described, an equivalent external force field is used to describe the acoustic source generation in the fluid[16].

Aero acoustic analogy

$$\frac{\partial^2 \rho'}{\partial t^2} - c_0^2 \frac{\partial^2 \rho'}{\partial x^2}$$

$$= \frac{\partial^2}{\partial x_i x_j}(T_{ij}H(f)) + \frac{\partial}{\partial x_i}(\sigma'_{ij}\delta(f)\frac{\partial f}{\partial x_j}) + \frac{\partial}{\partial t}(\rho_0 V_{si}\delta(f)\frac{\partial f}{\partial x_i}) \tag{3.8}$$

Derivation:
Continuity Equation

$$\frac{\partial \rho}{\partial t} + \nabla \cdot (\rho V) = 0 \tag{3.9}$$

Momentum Equation

$$\rho \frac{DV}{Dt} = -\nabla P + f \tag{3.10}$$

$$\rho \frac{\partial V}{\partial t} + \rho V \cdot \nabla V = -\nabla P + f \tag{3.11}$$

Rearranging Eq.(3.11)

$$\frac{\partial(\rho V)}{\partial t} + \nabla \cdot (P + \rho V V) = f \tag{3.12}$$

By taking time derivative of mass conservation and subtracting divergence of the momentum equation.

$$\frac{\partial^2 \rho}{\partial t^2} + \frac{\partial}{\partial t}(\nabla \cdot \rho V) = 0 \tag{3.13}$$

$$\nabla \cdot \left(\frac{\partial \rho V}{\partial t}\right) + \nabla \cdot (\nabla \cdot (P + \rho V V)) = \nabla \cdot f \tag{3.14}$$

$$\frac{\partial \rho}{\partial t} = -\nabla \cdot (\rho V) \tag{3.15}$$

18

$$\frac{\partial^2 \rho}{\partial t^2} - \nabla^2 (P + \rho V_i V_j) = \nabla \cdot f \tag{3.16}$$

$$\nabla \cdot \left(\frac{\partial \rho V}{\partial t} \right) = \nabla \cdot (\nabla \cdot (P + \rho V V)) + \nabla \cdot f \tag{3.17}$$

$$\frac{\partial^2 \rho}{\partial t^2} = \frac{\partial^2}{\partial x_i x_j} (P + \rho V_i V_j) \tag{3.18}$$

$$\sigma_{ij} = P \delta_{ij} - P_{ij} \tag{3.19}$$

$$\frac{\partial^2 \rho}{\partial t^2} = \frac{\partial^2}{\partial x_i x_j} (P \delta_{ij} - \sigma_{ij} + \rho V_i V j) + \frac{\partial f}{\partial x_j}$$

Add $\frac{1}{c_0^2} \frac{\partial^2 P'}{\partial t^2}$ on both side

$$\frac{\partial^2 \rho}{\partial t^2} + \frac{1}{c_0^2} \frac{\partial^2 P'}{\partial t^2} = \frac{\partial P \delta_{ij}}{\partial x_i x_j} + \frac{1}{c_0^2} \frac{\partial^2 P'}{\partial t^2} - \frac{\partial^2}{\partial x_i x_j} (\sigma_{ij} - \rho V_i V j) + \frac{\partial f}{\partial x_i} \tag{3.20}$$

$$\frac{1}{c_0^2}\frac{\partial^2 P'}{\partial t^2} - \frac{\partial^2 P'}{\partial x_i^2} = \frac{\partial^2}{\partial x_i x_j}(\rho V_i V j - \sigma_{ij}) - \frac{\partial f_i}{\partial x_j} + \frac{\partial^2}{\partial t^2}\left(\frac{P'}{c_0^2} - \rho\right) \qquad (3.21)$$

Eq.(3.21) shows that general sound can regarded as generated by three source distribution. This idea is illustrated in figure 3.5 in which we consider waves generated by a boat on the water surface.

- Acoustic quadruple source of strength density T_{ij} .

- This is supplemented by surface distribution of acoustic dipole source of strength density $P_{ij}n_j$.

- If surface moving volume displacement effect responsible for monopole effect.

When a person jumps up and down in the boat, he produces an unsteady volume injection and this generates a monopole wave field around the boat. When two persons on the boat play with a ball, they will exert a force on the boat each time they throw or catch the ball. Exchanging the ball results into an oscillating force on the boat. This will make the boat translate and this generates a dipole wave field. We could say that two individuals fighting with each other is a reasonable model for a quadruple[13]. This indicates that quadruples are in general much less efficient in producing waves then monopoles or dipoles. This will indeed appear to be the case. It is often stated that Lighthill has demonstrated that the sound produced by a free turbulent isentropic flow has the character of a quadruple. A better way of putting it is that since in such flows there is no net volume injection due to entropy production nor any external force field, the sound field can at most be a quadruple field.

3.5.2 Curle's formulation and Fowcs williams -Hawking formulation

The integral formulation of Lighthills analogy can be generalised for flows in the presence of wall section $''S''$ whereas formulation of Ffowcs Williams and Hawkings allows the use of a moving control surface $''S(t)''$.

3.5.3 Derivation

Continuity Equation:
$$\frac{\partial(\rho - \rho_0)}{\partial t} + \frac{\partial(\rho u_i)}{\partial y_i} = 0 \qquad (3.22)$$

Momentum Equation:
$$\frac{\partial(\rho u_i)}{\partial t} + \frac{\partial(\rho u_i u_j + P_{ij})}{\partial y_i} = 0 \qquad (3.23)$$

Where P_{ij} is compressive stress tensor

Replace $\rho - \rho_0$ as $\tilde{\rho}$ Continuity equation valid for entire unbounded region is given with Heaviside function $H(x)$

Heaviside function defined as

$$H(x)=\begin{cases} 0 \text{ if } x < 0 \\ \text{undefine } x = 0 \\ 1 \text{ if } x > 0 \end{cases}$$

Relation between dirac delta function and Heavside function given as

$$\frac{dH}{df} = \delta(f)$$

$$\frac{\partial(\tilde{\rho}H)}{\partial t} + \frac{\partial((\rho u_i)H)}{\partial y_i} = H\left[\frac{\partial \tilde{\rho}}{\partial t} + \frac{\partial(\rho u_i)}{\partial y_i}\right] + \tilde{\rho}\frac{\partial H}{\partial t} + \rho u_i \frac{\partial H}{\partial y_i} + \rho_0 u_i \frac{\partial H}{\partial y_i} - \rho_0 u_i \frac{\partial H}{\partial y_i} \qquad (3.24)$$

$$\frac{\partial H}{\partial t} + \rho u_i \frac{\partial H}{\partial y_i} = \delta(f)\frac{\partial f}{\partial t} + u_i \delta(f)\frac{\partial f}{\partial y_i}$$

$$= \delta(f)\left(\frac{\partial f}{\partial t} + u_i \frac{\partial f}{\partial y_i}\right) \qquad (3.25)$$

$$= \delta(f)\left[\frac{\partial f}{\partial y_i}\frac{\partial y_i}{\partial t} + u_i \frac{\partial f}{\partial y_i}\right] \qquad (3.26)$$

$$= \delta(f)\left[u_i - v_i\right]\frac{\partial f}{\partial y_i} = \delta(f)|\nabla f|(u_n - v_n) = 0 \qquad (3.27)$$

v_i velocity of body and because of no penetration $u_n - v_n = 0$ where n normal component of the body

$$\frac{\partial(\tilde{\rho}H)}{\partial t} + \frac{\partial((\rho u_i)H)}{\partial y_i} = \rho_0 u_i \delta(f)\frac{\partial f}{\partial y_i} = \rho_0 u_i \delta(f)|\nabla f| = \rho_0 u_n \delta(f)|\nabla f| \qquad (3.28)$$

Right hand source terms indicate following point

1. First term $\frac{\partial}{\partial t}\left[\rho_0 v_n |\nabla f|\delta(f)\right]$ is monopole source which also known as thickness noise.

2. Second term $\frac{\partial}{\partial y_i}\left[P_{ij}\delta(f)\frac{\partial f}{\partial y_j}\right]$ is dipole source term which responsible for broadband noise - Blade vortex interaction noise.

3. Third term $\frac{\partial^2}{\partial y_i \partial y_j}\left[P_{ij} + \rho u_i u_j - c^2 \tilde{\rho}\delta_{ij}\right]$ is well known lighthill tensor T_{ij} responsible for quadruple source .

4. Thickness noise : Noise created due to motion of the surface in normal direction each element can be consider as piston acting on flux with speed v_n.

5. Loading noise: Noise created due to pressure distribution on the surface. It includes blade vortex interaction broadband noise.

Chapter 4

Numerical Modelling and Solution

4.0.4 Turbulence Model

Because of the complexity of fluid turbulence, currently there is no single turbulence model which is valid for all turbulent phenomena. However, the k -ϵ model is widely used in industry due to its stability and convergence.

4.0.5 Mathematical Model of Turbulence

The $k-\epsilon$ model is a semi-empirical turbulence model. The initial idea of developing this model was to improve the mixing-length hypothesis and to avoid prescribing the turbulence length scale algebraically. There are two equations in this model, the k equation and the ϵ equation. k represents turbulence kinetic energy and ϵ represents the dissipation rate. They can be obtained by solving the following transport equations.

$$\frac{\partial(\rho k)}{\partial t} + \frac{\partial(\rho u_i k)}{\partial x_i}$$

$$= \frac{\partial}{\partial x_i} \left[\left(\mu + \frac{\mu_t}{\sigma_k} \right) \frac{\partial k}{\partial x_i} \right] + \mu_t \left(\frac{\partial u_i}{\partial x_j} + \frac{\partial u_j}{\partial x_i} \right) \frac{\partial u_i}{\partial x_j} - \rho\epsilon \tag{4.1}$$

$$\frac{\partial(\rho \epsilon)}{\partial t} + \rho u_k \frac{\partial k}{\partial x_k}$$

$$= \frac{\partial}{\partial x_k} \left[\left(\mu + \frac{\mu_t}{\sigma_\epsilon} \right) \frac{\partial \epsilon}{\partial x_k} \right] + \frac{c_1 \epsilon}{k} \mu_t \left(\frac{\partial u_i}{\partial x_j} + \frac{\partial u_j}{\partial x_i} \right) \frac{\partial u_i}{\partial x_j} - c_2 \rho \frac{\epsilon^2}{k} \tag{4.2}$$

μ_t is called turbulent viscosity and defined as

$$\mu_t = c_\mu \rho \frac{\epsilon^2}{k} \tag{4.3}$$

The constants $c_1, c_2, c_\mu \sigma_k, \sigma_\epsilon$ are respectively 1.44, 1.92, 0.09, 1.0, and 1.3. However, with the given values, the model is only suitable for high Reynolds flow, which works well if the flow is fully developed and is sufficiently spaced from wall boundaries. To improve the performance of the model in the near wall fields, wall functions can be used to model boundary effects.

4.0.6 Large Eddy Simulation

The Large Eddy Simulation (LES) turbulence model is a hybrid approach. In LES, the large motions are directly computed but the small eddies are usually approximated using a model [5]. It is the most widely used model in academia, but it is still not popular in industrial applications. One of the reasons is that the near wall region needs to be represented with an extremely fine mesh not only in the direction perpendicular to the wall but also parallel with the wall. For this reason, LES is not recommended with flows with strong wall boundary effects. In other words, the flow should be irrelevant to the wall boundary layers. Another disadvantage of LES turbulence model is the excessive computational power needed due to the statically stability requirement. Generally, the LES solver requires long computation time to reach a stastically stable state. Therefore a substantially long preparation time is needed for successful run of LES .

The main idea of the LES formulation is to separate the Navier-Stokes equations into two parts, a filtered part and a residual part. Filtering in LES is a mathematical operation separates a range of small scales from the Navier-Stokes equations solution. The large scale motions are resolved in the filtered part while the small scale motions are modeled in the residual part. The large scale motions are strongly influenced by the geometry and boundary conditions. The small scale motions are determined by the rate of energy transport from large-scale eddies and viscosity. Well documented explanations of filtered Navier-Stokes equations can be found in many turbulence modeling textbooks, and the subgrid-scale (SGS) turbulence model is used to model the near-wall regions. Using the SGS model, the SGS stress can be found using $\tau_{ij} - \frac{1}{3}\tau_{kk} = -2\mu_t \bar{S}_{ij}$

where μ_t represent the SGS turbulent viscosity and $\bar{S}_{ij}$ is the rate of strain tensor for the resolved scale defined by :

$$\bar{S}_{ij} = \frac{1}{2}\left(\frac{\partial \bar{u}_i}{\partial x_j} + \frac{\partial \bar{u}_j}{\partial x_i}\right) \tag{4.4}$$

4.0.7 Acoustic Numerical Solution

There are two major types of numerical methods in acoustics: the boundary element method (BEM) and finite element method (FEM). Although noise control engineering primarily depends on measurement and experience, numerical methods have been used to predict noise in the early design stage as a means to lower the cost of design by increasing design efficiency . Normally, acoustic FEM is used to solve interior problems, but nowadays FEM can be used to solve acoustic radiation problems with the advent of infinite elements[3]. The Helmholtz equation is the governing equation for linear acoustics and can be expressed as

$$\nabla^2 p + K^2 p = 0 \tag{4.5}$$

Where p is the sound pressure and K is the wavenumber.

4.0.8   Fan curve and fan laws

To evaluate a fan with respect to its ability to transport an air volume, fan curves are used. To make things clearer one can think about a circuit, where the fan is the source that produces the pressure difference $\Delta P = P_1 - P_0$ to overcome the resistance of the system. Instead of a current an airflow rate $Q = \frac{m^3}{s}$ is circulating. The illustration of this analogy is shown in Figure 4.1(a). The BS 848 standards (1980) defines the fan static pressure rise as the static pressure at the outlet minus the total pressure at the inlet. Figure 4.1(b) shows general fan curve, x-axis ordinate represent
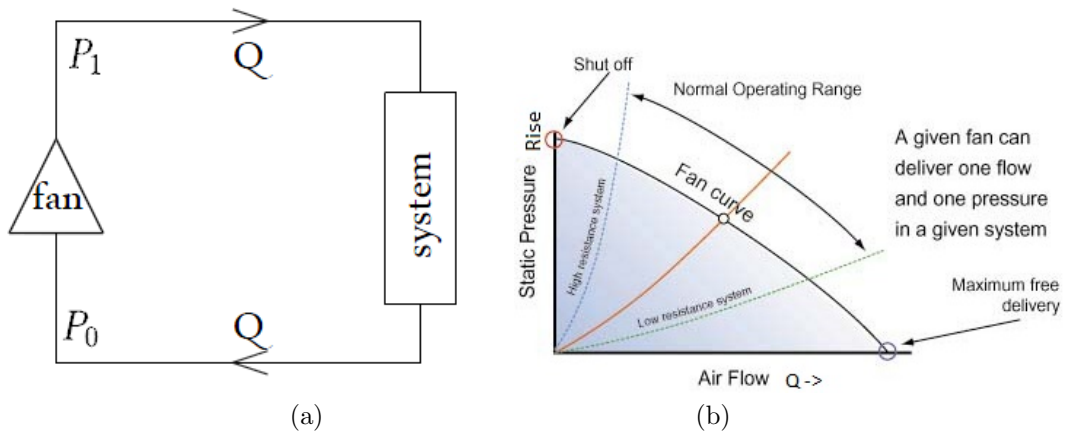

Figure 4.1: (a) Electrical analogy for fan curve [3](b)typical fan curve

volume flow rate and y-axis represent static pressure difference. The fan curve is the black dark line which cuts the coordinate system twice. The cut with the x-axis gives the maximum airflow through the fan. Here the fan is at maximum kinetic energy. The cut with the y-axis denotes the shut-off point. The fan curve can be created if a prototype is available and is therefore provided by the fan manufacturer. The fan curve can also be computed by using CFD analysis. This is done in this thesis. Figure 4.2(a) shows fan curve generated from CFD data. Whereas Figure 4.2(b) shows normalized fan curve. By using curve fitting technique pressure rise at shut off point can be calculated. Centrifugal fans generally fallow parabolic curve.
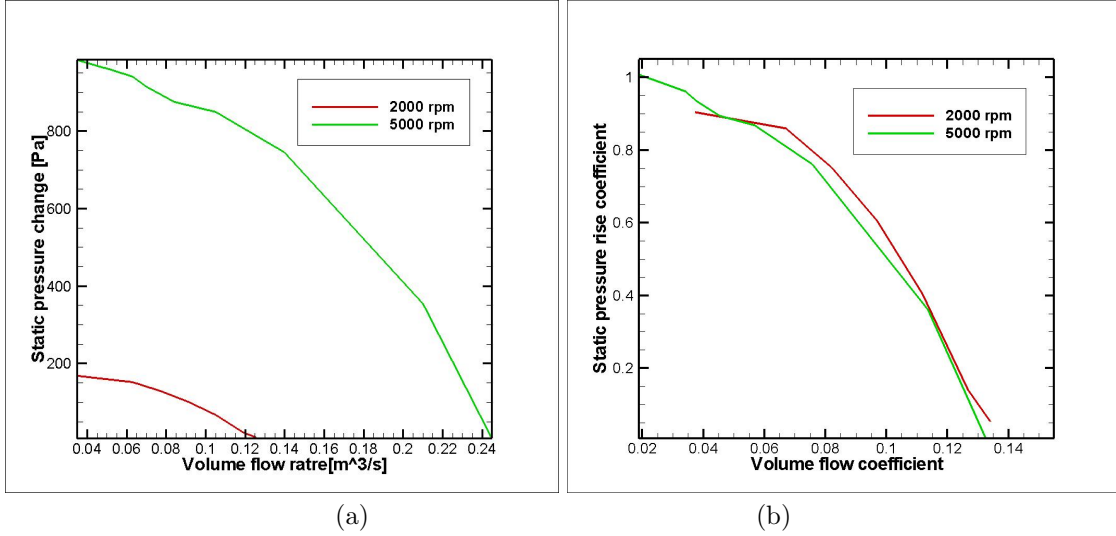
Figure 4.2: (a)fan curve from CFD solution for centrifugal fan(b)Normalized fan curve for centrifugal fan

A guideline for effects of different variable changes between geometrically similar fans is provided by fan laws. Such laws have a solid theoretical background and have also been determined experimentally By looking at two geometrically similar fans with constant speed and air density one can conclude parameter influences. The two different diameters,D_1 and D_2, can be related with other parameters in the following way:

$$\frac{P_1}{P_2} = \left(\frac{D_1}{D_2}\right)^2$$

$$\frac{Q_1}{Q_2} = \left(\frac{D_1}{D_2}\right)^3$$

P denotes the pressure and Q is the airflow through the different fans. The first law can be easily explained in terms of airflow rate and the centrifugal force. It grows in radial direction with the square of the distance to the rotation axis. This force is then balanced with the pressure, which is zero close to the rotation axis and increases in outwards direction.

$$\frac{\partial P}{\partial r} = \rho r \omega^2$$

After integration we can calculate pressure rise at shut off point. Sample calculation:

$$\Delta P_{max} = \frac{\rho r_0^2 \omega^2}{2} = \frac{1.27 \times \left(\frac{0.15}{2}\right)^2 \times \left(\frac{2000}{60}\right)^2}{2} = 156.679 \ Pa$$

Table 4.1 shows very small difference in numerical and theoretical shut off point calculation .These results shows validation of numerical model.

Non dimensional aerodynamics performance parameter defined in term of ϕ_r and ψ_{st}. ϕ_r is non-dimensional volume flow coefficient and ψ_{st} is static pressure rise coefficient defined as

$$\phi_r = \frac{Q}{\pi^2 d^2 bn}$$

25

Table 4.1: Comparison of numerical results with theoretical values at shutoff point

RPM	Theoretical ΔP_{max}	Numerical ΔP_{max}	%Error
2000	156.679	154.92	1.12
5000	979.24	936.58	4.35
3000	69.635	67.189	3.51

$$\psi_{ts} = \frac{2\Delta P_{ts}}{\pi^2 d^2 \rho n^2}$$

respectively where d is diameter ,b is width of blade,n is number of rotation per second and Q is volume flow rate .

Sample calculation:

$$\phi_r = \frac{Q}{\pi^2 d^2 bn} = \frac{0.035}{1.27 \times \pi^2 \times 0.15^2 \times 0.1 \times 33.33} = 0.037$$

$$\psi_{ts} = \frac{2\Delta P_{ts}}{\pi^2 d^2 \rho n^2} = \frac{2 \times 141.63}{\pi^2 \times 0.15^2 \times 1.27 \times 33.33^2} = 0.904$$

Table 4.2 and 4.3 gives non-dimensional value for fan curve at 2000 RPM and 5000 RPM advan-

Table 4.2: Simulated centrifugal fan curve data at speed of 2000 rpm

$\Delta P_{st}(Pa)$	Q(m3/s)	ψ_{st}	ϕ_r
141.630	0.035	0.904	0.037
134.52	0.063	0.859	0.067
117.686	0.077	0.751	0.081
94.830	0.091	0.605	0.096
63.330	0.105	0.404	0.111
21.955	0.119	0.140	0.119
8.2015	0.126	0.140	0.126

tage of non-dimensionalized fan curve is that it can applicable for any geometrically similar fan.

Table 4.3: Simulated centrifugal fan curve data at speed of 5000 rpm

$\Delta P_{st}(Pa)$	$Q(m3/s)$	ψ_{st}	ϕ_r
985.383	0.035	1.007	0.018
963.562	0.049	0.984	0.026
940.402	0.063	0.961	0.034
914.048	0.07	0.934	0.037
875.526	0.084	0.894	0.045
849.088	0.105	0.867	0.056
744.584	0.14	0.761	0.075
353.244	0.21	0.361	0.113
6.491	0.245	0.006	0.132

4.1 Fan noise simulation approach

4.1.1 Computational Aero acoustics

Usually in an aero acoustic problem, there are four aspects to consider: the sound wave and the acoustic medium, sources, and the receiver. The medium in aero acoustic problems is air or a gas mixture. The sources are the pressure fluctuations due to vortex shedding and turbulence. The receiver can be microphones (or field points in a simulation) or, in reality, the human ears. There are three primary aero acoustic simulation approaches: computational aero acoustics (CAA), CFD-sound propagation solver coupling, and broadband noise source models. The aero acoustic simulation in a CFD-sound propagation solver coupling process is based on variables such as the pressure and density fields computed by a CFD solver during transient flow simulation. Figure 9 shows the solution process of this solver coupling approach. The aero acoustic solver will read in the transient CFD solution data and compute the aero acoustic sources in the time domain. Acoustic simulation can be done either in frequency domain or time domain based on problem. The current problem considered to be in frequency domain. Then a Fast Fourier Transform is conducted in order to obtain the source data in the frequency domain. After the frequency domain sources are computed, an acoustic simulation can be performed
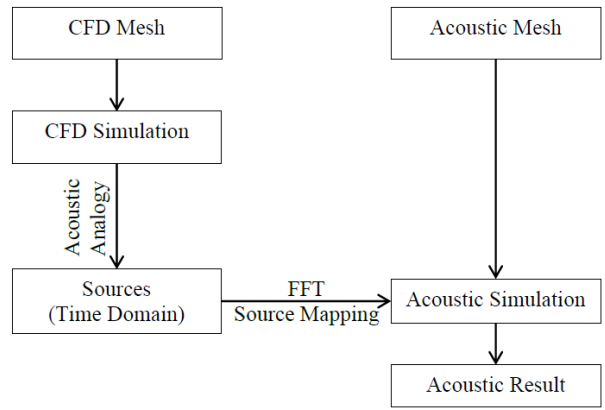
Figure 4.3: CFD-Sound Propagation Solver coupling solution process

4.1.2 Geometry

Centrifugal fan CAD model created in commercial software SOLIDWORKS[17] as shown in Figure 4.4 . Figure 4.5 is horizontal sectional view. Fan consist of 12 blades. Inlet showed by red color whereas outlet showed by orange color. Horizontal section view in Figure 4.5 gives dimension and this section used to analyses results in rest of the thesis. Yellow region showed in figure 4.4 transparent view is rotating part. There is 20 mm minimum clearance between blades and external body.
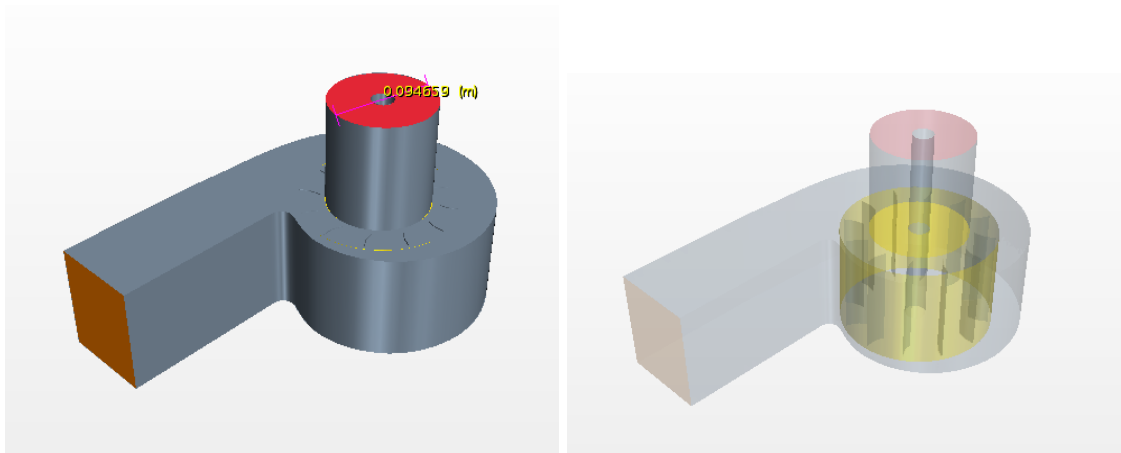
Figure 4.4: CAD Model of centrifugal fan with inlet and outlet duct configuration.
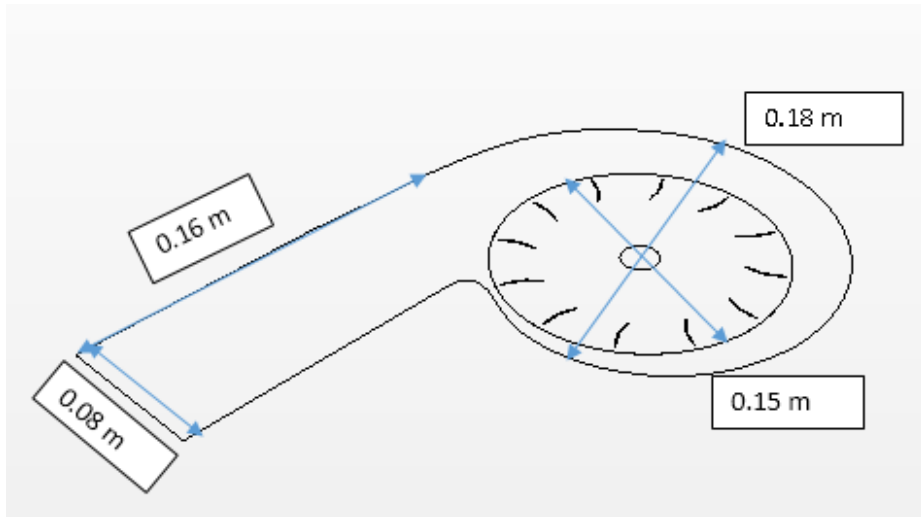
Figure 4.5: Horizontal slice of geometry

4.1.3 Grid Independent study

Advantages of polyhedral mesh:
Polyhedral meshes offer the same automatic meshing benefits as tetrahedral meshes, being easy and efficient to build, while overcoming their disadvantages such as limited stretching and poor gradient approximation. A major advantage of polyhedral cells is that they have many neighbors (typically of the order of 10), so gradients can be much better approximated (using linear shape functions and the information from nearest neighbors only) compared with tetrahedral cells.

Polyhedral cells are especially beneficial for handling re-circulating flows. Tests [STAR CCM+][18] have shown that, for example, in the cubic lid-driven cavity flow, fewer polyhedral cells are needed to achieve a specified accuracy than even Cartesian hexahedral cells (which would be expected to be optimal for rectangular solution domains). This can be explained by the fact that, for a hexahedral cell, there are three optimal flow directions which lead to the maximum accuracy (normal to each of the three sets of parallel faces); for a polyhedron with 12 faces, there are six optimal directions which, together with the larger number of neighboring cells, leads to a more accurate solution with a lower cell count. Comparisons in many practical tests have verified that, with polyhedral meshes, approximately four times fewer cells, half the memory, and a tenth to a fifth of computing time is required to achieve a solution as compared to a tetrahedral mesh with the same level of accuracy. In addition, convergence properties are much better in computations on polyhedral meshes, where the default solver parameters usually do not need to be adjusted.

By definition, a mesh-converged solution means, to make the mesh fine in each spatial dimension and run the simulation again. If the solution for the original and the refined mesh are identical, or nearly so, the solution can be assumed to be Mesh-converged. Here to study grid independency three mesh compared with 3mm, 4 mm and 5mm base size as shown in figure 4.7 and 4.8.Meshing has been done in commercially available software STAR CCM+.

Polyhedral 4 mm base size is operating mesh which is 45.20% coarse and 33.76% finer than 3 mm and 5 mm base size mesh.There are two region in given mesh rotating and stationary. Rotating
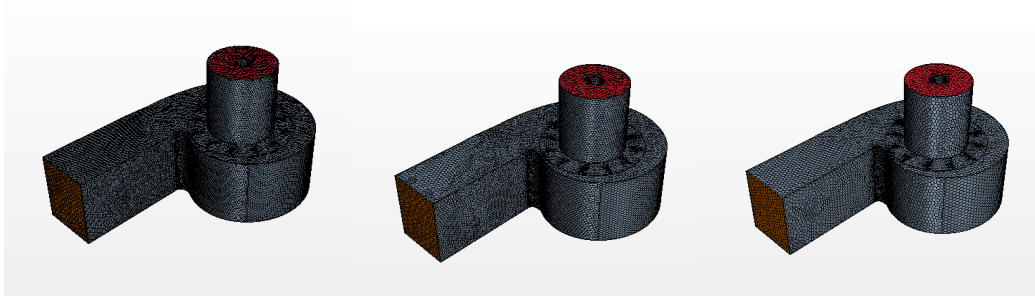
Figure 4.6: 3mm base size Mesh (410847 cells) , 4mm base size Mesh (225121 cells),5mm base size Mesh (149117 cells) respectively.
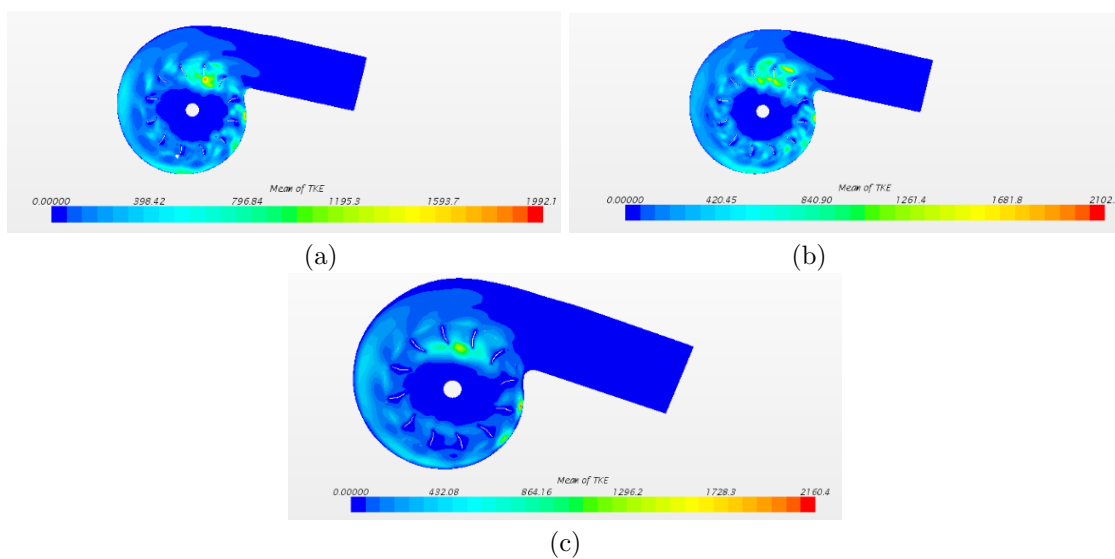

Figure 4.7: Turbulent kinetic energy results for (a)5mm base size (b)3 mm base size and (c) 4 mm base size

region mesh is more finer compared to stationary region. Important scalar quantity tangential velocity, static pressure rise and turbulent kinetic energy listed in table 4.4. Numerical solutions compared in table 4.4 shows grid independency.

Table 4.4: Grid Independent study

Base Size	Cells	Max $V_t(m/s)$	$\Delta P(Pa)$	Max TKE (Joule)	%Error
5 mm	149117	18.705	146.76	1992.1	3.2 and 5.2
3mm	410847	17.712	142.14	2102.3	Ref
4 mm	225121	18.532	144.465	2160.7	1.6 and 2.7

4.2　Numerical solution

Numerical Modelling: The analysis of CFD problems generally involve three steps:

1. Discretization of the flow domain

2. Setting up and initiating the flow computation

3. Visualizing the results

RANS equation solved with following turbulence model.

1. $k - \epsilon$ turbulent model

2. $k - \omega$ turbulent model

3. Spart-alahamas turbulent model

4. LES turbulent model

Acoustic overall power calculation done with these CFD solution and compared in table 4.5.

Table 4.5: Comparison predicted total sound power levels by using different turbulence models in CFD

Turbulence Model	Overall Noise Prediction (dB)
K-ϵ	105.02
K-ω	105.45
Spart-alahamas	105.92
LES	103.73

From equation 2.1

$$L_w = K_w + 70logD + 50logN + C$$

$$= 85 + 70 \times log(0.15) + 50 \times log(\frac{2000}{60}) = 103.47dB + C$$

Results shows LES CFD analysis gives better results than rest of turbulence model. Unsteady NavierStokes equations solved with MRF mesh considering incompressible, segregated flow with
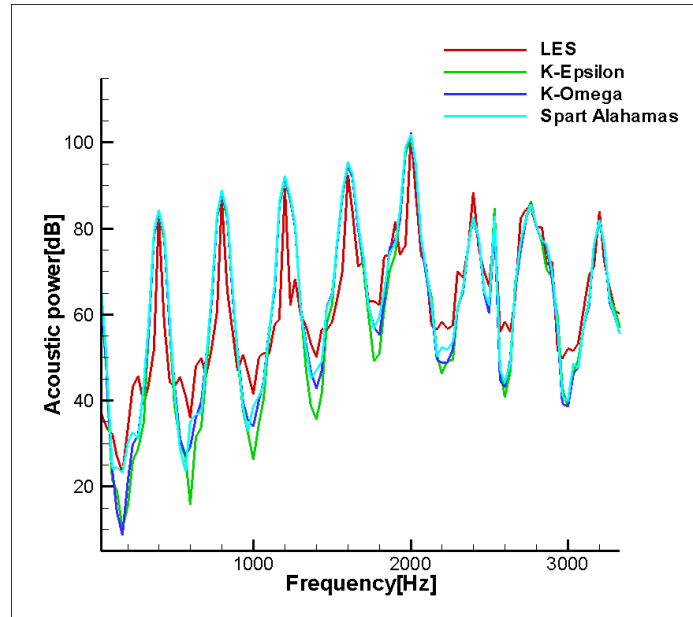
Figure 4.8: Comparison predicted total sound power levels by using different turbulence models in CFD

implicit scheme. Implicit scheme numerical more stable than explicit scheme but it can't unconditionally stable so we need to consider time step which satisfy courant number criteria(CFL no.<1) In this thesis, it is 2e-5 which satisfy CFL criteria and according to Nyquist criteria can give sound pressure level up to 25KHz.

Detailed step for CFD analysis mentioned in appendix.

Parameters :

Gas properties:

Density =1.18 kg/m3

Dynamic viscosity =1.85E-5 N-s/m2

CFD Boundary condition :

Inlet Velocity = 11 m/s

Blade rotation = 2000 rpm

Pressure Outlet = atmospheric pressure

Acoustic Boundary condition :

Pressure at inlet and outlet is equal to atmospheric pressure.

Velocity of sound =340 m/s

Figure 4.9 shows Reynolds number and velocity magnitude contour, it indicate wherever velocity magnitude is high, Reynolds number is also high.

4.2.1   Wave propagation using Boundary Element Method

Unsteady turbulent model solved with large eddy simulation and MRF mesh considering incompressible, segregated flow and implicit scheme. Pressure data on blade surface from CFD analysis
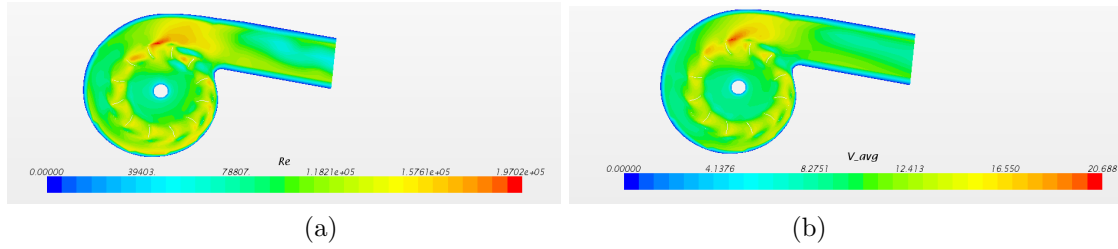
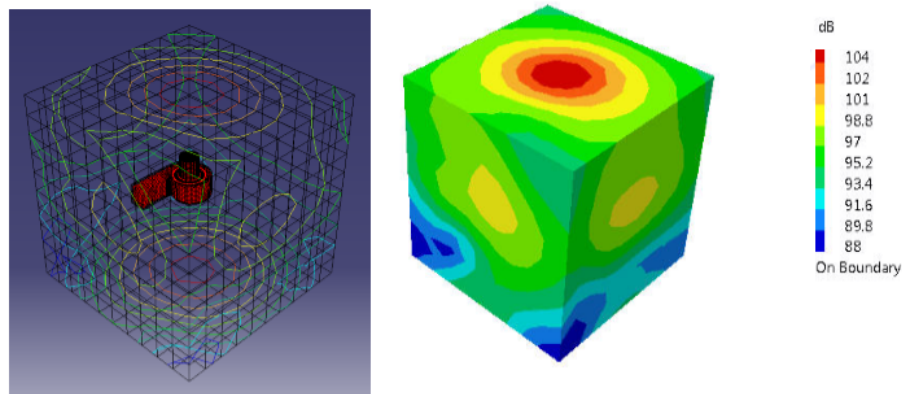Figure 4.9: (a)Reynolds's number with diameter as characteristic length (b) Velocity vector contour

Figure 4.10: Acoustic pressure autopower contour(dB) at 2000 Hz(rotational speed,2000 RPM)

used to find forces or acoustic source term in nonhomogeneous wave equation. After finding source term in wave equation, directivity contour plotted in $1m^3$ cubical field point as showed in Figure 4.10. Figure 4.10 shows monopole like source term at inlet condition. Whereas Figure 4.11 shows monopole and dipole like behavior at 500 Hz and 1000 Hz respectively. After plotting acoustic power spectrum, it found that 5th BPF harmonic is dominating. Overall acoustic power level is 103.73 dB and compared with empirical values as given in Eq (2.1). The values are in close agreement.figure 4.13 shows sectional view acoustic pressure distribution at different section at peak frequency 2000 Hz. After doing acoustic modal analysis it found that it is effect of large bottom circular duct.
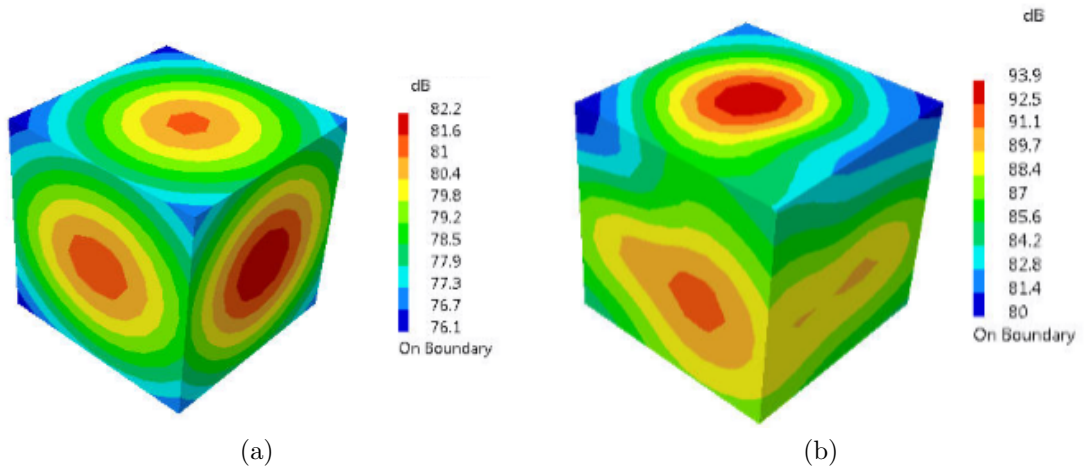
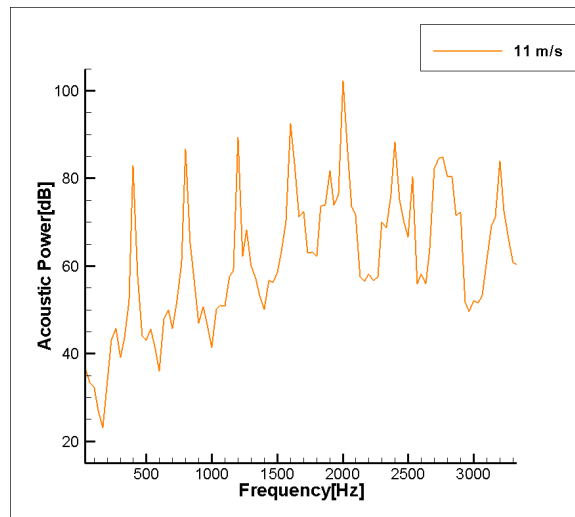Figure 4.11: Acoustic pressure autopower contour(dB) at (a)500 Hz and (b)1000 Hz

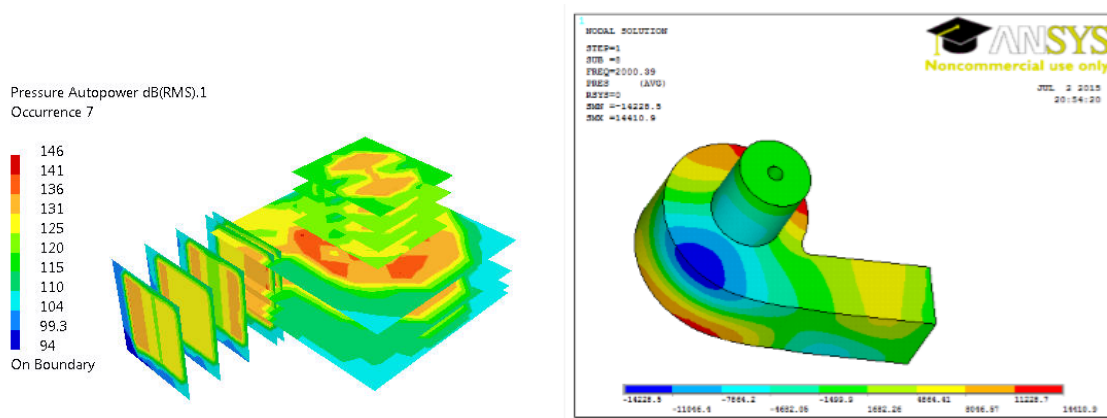Figure 4.12: Spectrum of centrifugal fan rotating at speed of 2000 rpm.

Figure 4.13: Acoustic modal analysis

Chapter 5

Parametric study

As earlier mention, LES turbulence model predict noise close to empirical prediction. so, LES turbulence model continued for rest of parametric study.

5.1 Variation of Inlet Velocity

As we have seen in Chapter 4, volume flow rate to create Fan curve. To get optimum performance point (less noisy), acoustic power vs volume flow rate plot have created. Prior to that Velocity, turbulent kinetic energy, vorticity contour plotted to observe fluid dynamics at rotational speed of 2000 RPM.

(a)   (b)
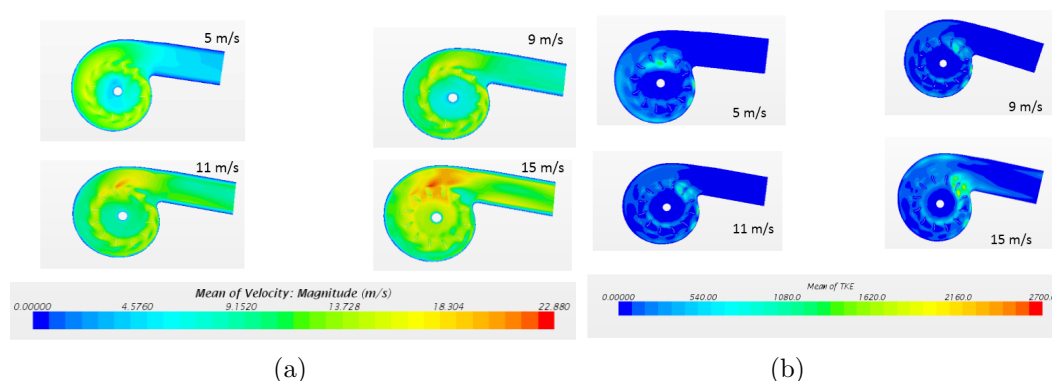
Figure 5.1: (a)Velocity Magnitude Contour (b) Turbulent Kinetic Energy contour for various inlet velocity condition

As shown in figure 5.1 (a) velocity magnitude is increasing with increasing inlet velocity. Figure 5.2 compare vorticity contour for various inlet velocity condition. It is maximum at cut off in all contour.

Figure 5.1 shows as turbulent kinetic energy increases leads to increment of total acoustic power. Intially overall acoustic power decreases and then increases.
Figure 5.3 and Figure 5.4 shows acoustic power at various frequencies and all peaks are associated
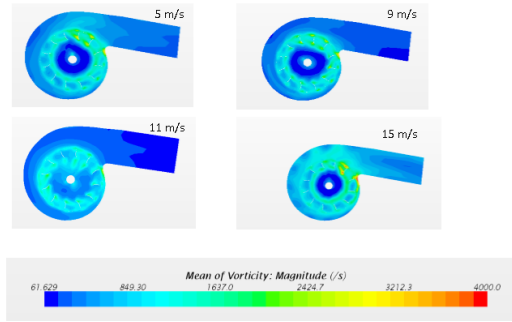
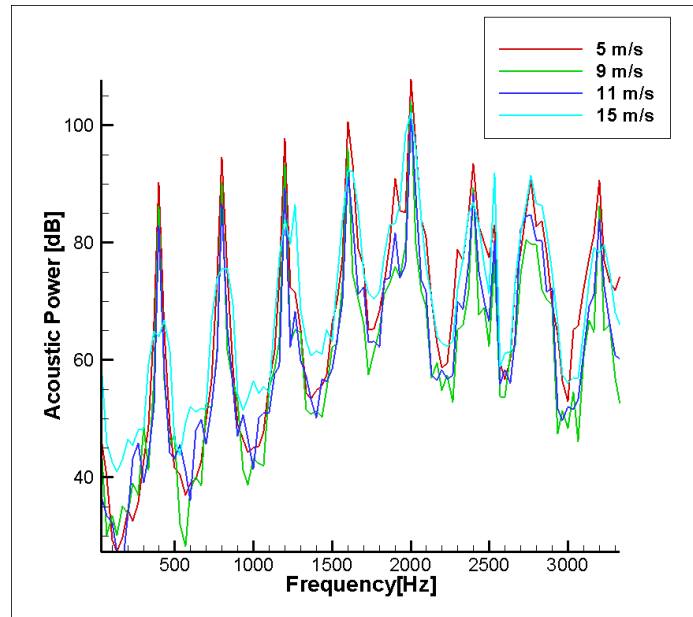Figure 5.2: Vorticity Magnitude Contour for various inlet velocity condition

Figure 5.3: Acoustic Power spectrum for various inlet velocity condition (rotationalspeed,2000 RPM)

with harmonics of blade passing frequency. In case of 2000 RPM, blade passing frequency is 400 Hz where as in 5000 RPM case it is 1000 Hz . Similiar parametric study have done for 5000 RPM. Same trend found as 2000 RPM.
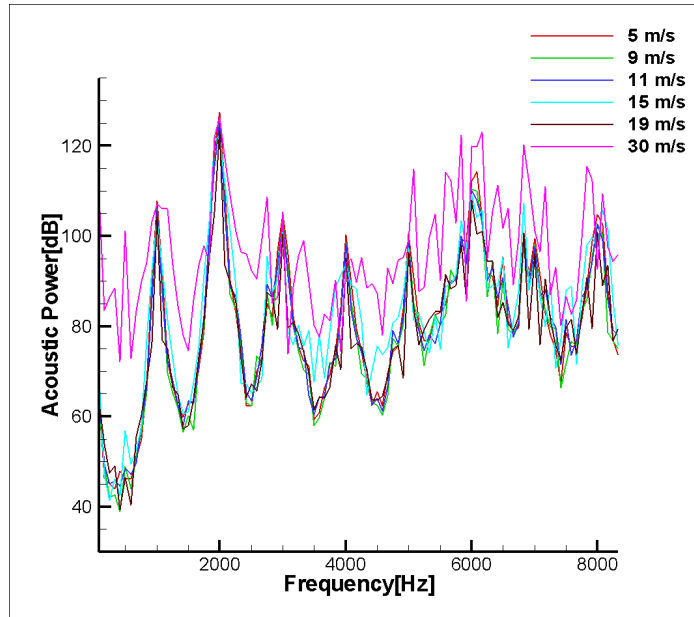
Figure 5.4: Acoustic Power for various inlet velocity condition (rotational speed, 5000 RPM)

5.2 Number of Blade Variation

Here two cases considered: .

1. Fan with six blades

2. Fan with twelve blades
   There is no particular relation between acoustic power and number of blades, but here acoustic power increased after reducing the number of blades. Turbulent kinetic energy (TKE) and vorticity contour plot values are increased as number of blades decreased. It can be observed from Figure 5.5
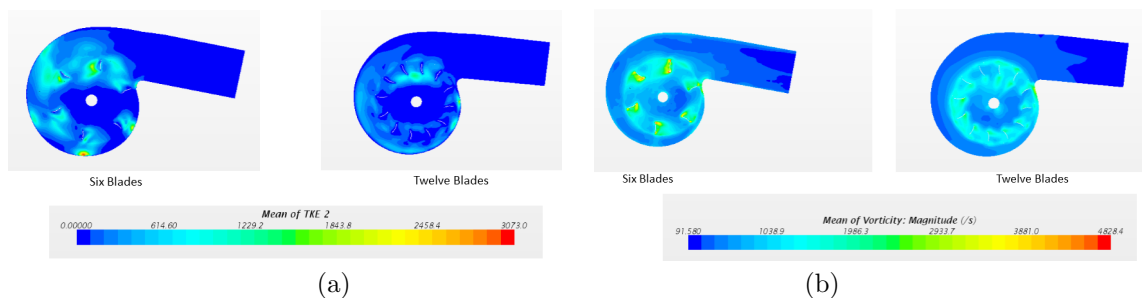

Figure 5.5: (a)TKE contour comparison (b) Vorticity contour comparison

In six blade case blade passing frequency (BPF) 200 Hz and its harmonics are dominating. Blade passing frequency defined as
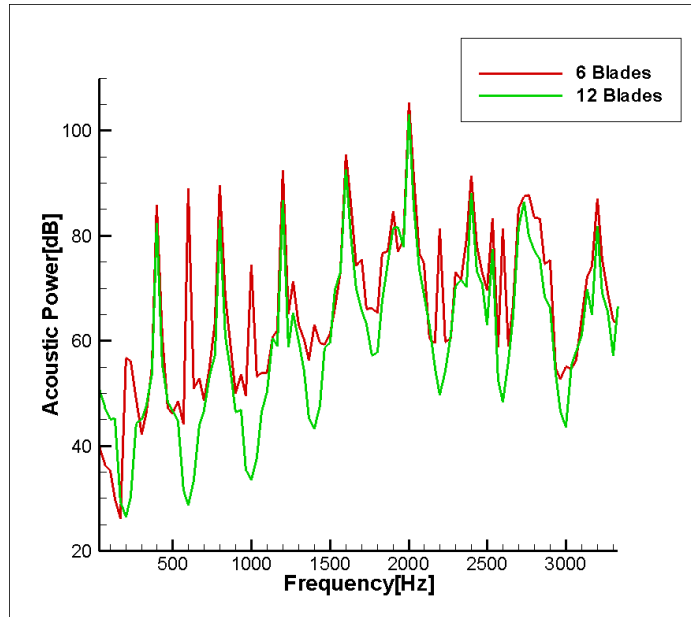
Figure 5.6: Acoustic Power(dB) comparison on cubical field point mesh

$$BPF = \frac{n \times N}{60} \tag{5.1}$$

Where as in 12 blades case, 400 Hz (BPF) and its harmonics are dominating.

5.3 Cut off radius variation

As we have seen earlier, most of the cases TKE was maximum at cut off radius so to observe effects of cut off radius on acoustic power this study has been done. Original geometry's cut off radius modified in commercial software SOLID WORKS.Modified geometry rescaled and mehing has been done in commercial available CFD software STAR CCM +. Figure 5.7 shows modified geometry similarly cut off radius modified to 15 mm , 25 mm and 30 mm.Figure 5.8 shows comparison of turbulent kinetic energy contour for various cut off radius.Figure 5.9 shows comparison of vorticity contour for various cut off radius.Figure 5.8 shows there is no specific trend for the turbulent kinetic energy initially it is increasing but later it is decreasing, it is because of initially both (blade tip and cut off radius) clearance and obstruction to flow increases later clearances increases but obstruction decreases.Similar trend found in term of vorticity magnitude contour and acoustic total power as showed in figure 5.9 and figure 5.10 respectively.Table 5.1 shows total acoustic power for various cut off radius. As turbulent kinetic energy initially it is decreasing and then it is increasing.
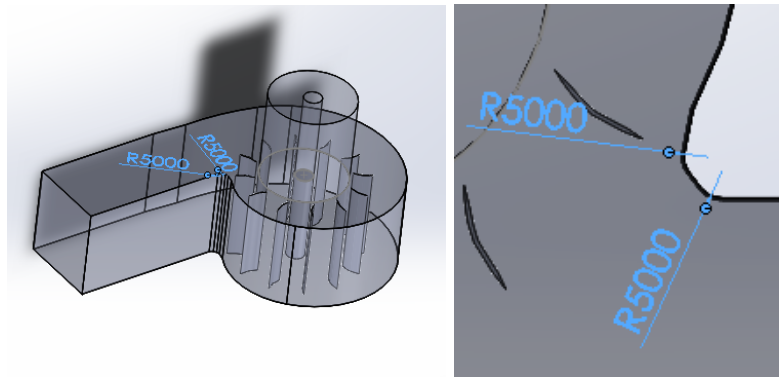

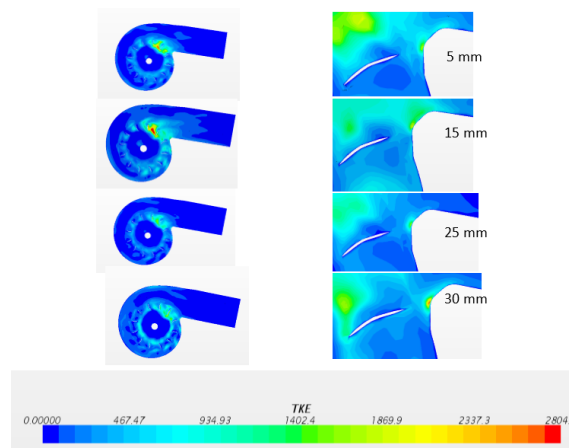Figure 5.7: Modified cut off radius geometry

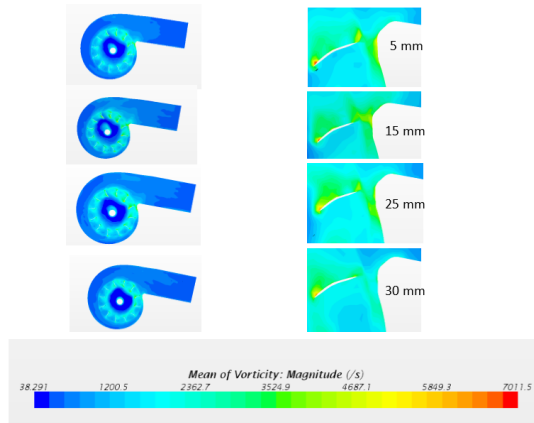Figure 5.8: Effect of cut off radius on TKE contour.

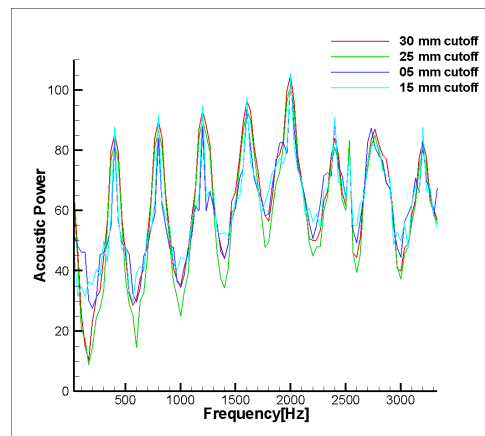Figure 5.9: Effect of cut off radius on vorticity magnitude contour.

Figure 5.10: Acoustic power for various cutoff radius

Table 5.1: Optimum operating condition for 2000 RPM

Cut off radius (mm)	Total acoustic power (dB)
05	106.81
15	105.05
25	104.60
30	107.71

Chapter 6

Conclusion

Developed a methodology for given centrifugal fan. Fan curve prediction and validation has done and from acoustic power calculation, it can be concluded that the LES turbulence model can predict tonal noise for given fan. Turbulent kinetic energy and vorticity magnitude shows a direct relation to overall acoustic power

Parametric study have done.

(a) Variation of inlet velocity: The optimum operating condition can find from Fan curve and acoustic power curve. Here Table 6.1 and Table 6.2 gives overall acoustic power for various volume flow rates. From figure 6.1 and 6.2 it can be seen that at 0.77 m3/s for 2000 RPM and 0.133 m3/s for 5000 RPM fan performance is less noisy.

(b) Variation of blade number: As the number of blades decreases noise increase because of increment in turbulent kinetic energy and vorticity magnitude.

(c) Variation of cut off radius: In acoustic point of view, there is a tradeoff between curvature blade clearance and cut off radius.

Thus, given methodology helps to get this operating point without creating prototype, so proposed method is an appropriate design tool during initial design studies.

Table 6.1: Optimum operating condition for 2000 RPM

Acoustic Power (dB)	Volume flow rate
109.98	0.035
105.36	0.063
103.73	0.077
106.06	0.105

Table 6.2: Optimum operating condition for 5000 RPM

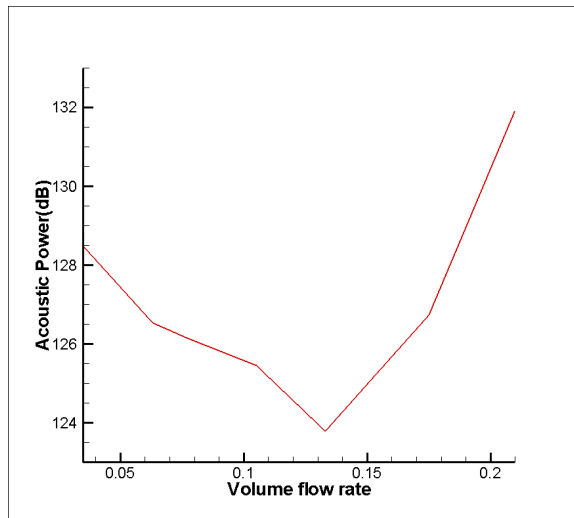| Acoustic Power (dB)	Volume flow rate
128.48	0.035
126.53	0.063
126.14	0.077
125.44	0.105
123.79	0.133
131.91	0.210

Figure 6.1: Acoustic power for various volume flow rate for 5000 RPM
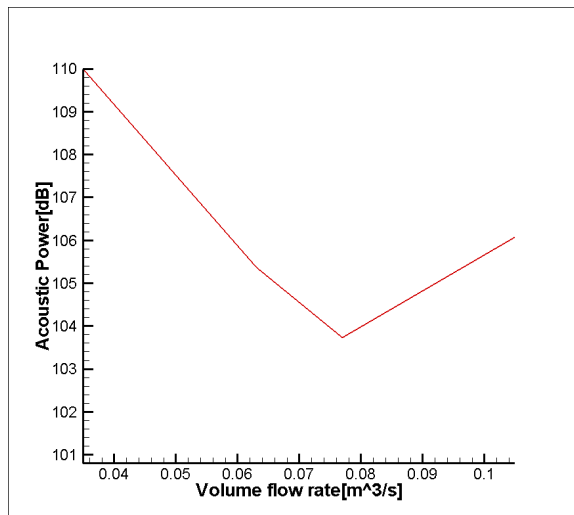

Figure 6.2: Acoustic power for various volume flow rate for 2000 RPM

References

[1] J. C. Hardin and S. L. Lamkin. Aeroacoustic Computation of Cylinder Wake Flow. *AIAA journal* 22, (1984) 51–57.

[2] J. Liu. Simulation of Whistle Noise Using Computational Fluid Dynamics and Acoustic Finite Element Simulation .

[3] L. C. Wrobel. The boundary element method, applications in thermo-fluids and acoustics, volume 1. John Wiley & Sons, 2002.

[4] F. Bakhtiari-Nejad, A. Rahai, and A. Esfandiari. A structural damage detection method using static noisy data. *Engineering Structures* 27, (2005) 1784–1793.

[5] D. C. Wilcox et al. Turbulence modeling for CFD, volume 2. DCW industries La Canada, CA, 1998.

[6] M. J. Lighthill. On sound generated aerodynamically. II. Turbulence as a source of sound. In Proceedings of the Royal Society of London A: Mathematical, Physical and Engineering Sciences, volume 222. The Royal Society, 1954 1–32.

[7] J. F. Williams and D. L. Hawkings. Sound generation by turbulence and surfaces in arbitrary motion. *Philosophical Transactions of the Royal Society of London A: Mathematical, Physical and Engineering Sciences* 264, (1969) 321–342.

[8] O. Singh, R. Khilwani, T. Sreenivasulu, and M. Kannan. Parametric study of centrifugal fan performance: Experiments and numerical simulation. *rN* 30, (1963) 2.

[9] M. Lowson. The sound field for singularities in motion. In Proceedings of the Royal Society of London A: Mathematical, Physical and Engineering Sciences, volume 286. The Royal Society, 1965 559–572.

[10] J. Wiedemann, G. Wickern, B. Ewald, and C. Mattern. Audi aero-acoustic wind tunnel. Technical Report, SAE Technical Paper 1993.

[11] I. Sharland. Sources of noise in axial flow fans. *Journal of Sound and Vibration* 1, (1964) 302–322.

[12] C. Morfey. Acoustic energy in non-uniform flows. *Journal of Sound and Vibration* 14, (1971) 159–170.

[13] D. CRIGHTON. Physical acoustics and the method of matched asymptotic expansions. *Physical Acoustics V11: Principles and Methods* 11, (2012) 69.

[14] G. Birkhoff. Formation of vortex streets. *Journal of Applied Physics* 24, (1953) 98–103.

[15] J. H. Lienhard. Synopsis of lift, drag, and vortex frequency data for rigid circular cylinders. Technical Extension Service, Washington State University, 1966.

[16] M. Fisher, P. Lush, and M. Harper Bourne. Jet noise. *Journal of Sound and Vibration* 28, (1973) 563–585.

[17] M. Lombard. Solidworks 2013 bible. John Wiley & Sons, 2013.

[18] M. Peric and S. Ferguson. The advantage of polyhedral meshes. *New corporate image for CD-adapco* .